View Article Online / Journal Homepage / Table of Contents for this issue
Dynamic Article Links

Journal of Materials Chemistry

Cite this: *J. Mater. Chem.*, 2011, **21**, 17938

www.rsc.org/materials

PAPER

Morphology-tunable architectures constructed by supramolecular assemblies of α-diimine compound: fabrication and application as multifunctional host systems†

Haiqing Li,[ab] Bijal K. Bahuleyan,[ac] Renjith P. Johnson,[a] Yury A. Shchipunov,[a] Hongsuk Suh,[d] Chang-Sik Ha[a] and Il Kim*[a]

Received 4th July 2011, Accepted 2nd September 2011
DOI: 10.1039/c1jm13081a

An α-diimine compound (DC) bearing multiple hydroxyl and amine groups presents excellent self-assembly behavior, yielding DC self-assemblies with tunable morphologies ranging from solid spheres, nanotubes and capsules *via* hydrogen bonds and π–π stacking interactions. These DC self-assemblies provide promising multifunctional hosts for varied metal species. As a typical example, Au nanoparticles are *in situ* generated and accommodated into both solid and hollow DC self-assemblies by one-pot and two-step fabrication processes, respectively, resulting in the formation of solid and hollow DC/Au hybrid nanostructures. Both solid and hollow DC self-assemblies also enable host Ni(II) ions to generate DC/Ni(II) catalysts for the efficient production of porous polyethylene (PE) beads consisting of numerous PE microspheres. Moreover, the yielded PE beads replicate the textural morphologies of the original DC/Ni(II) catalysts. These DC self-assemblies also might be further utilized to host varied metal species to fabricate versatile DC/metal nanoparticle (Ag, Pt, Pd, *etc.*) hybrids and porous polyolefin beads with desired morphologies.

Published on 12 October 2011. Downloaded by York University on 22/10/2014 13:03:49.

Introduction

Significant efforts have been devoted to the fabrication of diverse host systems with micro- and nanoscale size, as they provide some of the best means to obtain multifunctional materials with distinct and desired properties.[1] Supramolecular chemistry offers a powerful and convenient approach to prepare such fascinating host materials with well-defined architectures from small molecular building blocks, since the synthetic assemblies generally possess enormous internal cavities ranging from a few cubic angstroms to over a cubic nanometre.[2] Such supramolecular assemblies often rely on a variety of noncovalent interactions such as π–π interaction, hydrogen bonding, electrostatic attraction, metal–ligand coordination and their combinations to hold the subunits together.

Recent studies have demonstrated that the efficiency for guest-encapsulation strongly depends on the molecular composition and structure of the small building blocks owing to the following reasons: (1) functional components act as media to induce the formation of intermolecular non-covalent interactions; (2) the stereostructure of molecules together with (1) direct the stacking and growing fashions of building blocks into supramolecular assemblies, which not only determine the morphologies of final self-assembled architectures, but leads to the formation of internal cavities to facilitate guest species accommodation, transportation and exchange;[3] (3) functional moieties provide "active sites" to catch guest matter, forming novel hybrids with promising properties. Therefore, suitable molecular design of building blocks is of enormous significance to create promising supramolecular hosts. To date, based on diverse molecular compositions and structures of building blocks such as porphyrins,[4] bis(imidazol-1-ylmethyl)benzene,[5] *p*-phenylene-vinylene,[6] naphthalene,[7,8] *etc.*, a wide range of supramolecular host systems have been created and exhibit extensive catalytic, bio-imaging and photoelectrical functions by encapsulation of various functional guest species. However, most of those supramolecular hosts tend to lack multifunctional encapsulating capacity towards diverse guest matter, owing to the limited functions of building blocks. Especially for the multifunctional host systems

[a]*The WCU Center for Synthetic Polymer Bioconjugate Hybrid Materials, Department of Polymer Science and Engineering, Pusan National University, Busan, 609 735, Korea. E-mail: ilkim@pusan.ac.kr; Fax: +82 51-513-7720; Tel: +82 51 510 2466*
[b]*Australian Institute for Bioengineering and Nanotechnology, The University of Queensland, Brisbane, QLD, 4072, Australia. E-mail: h.li8@uq.edu.au*
[c]*Department of Chemistry, Tokyo Metropolitan University, Tokyo, 1920397, Japan. E-mail: kbijal@gmail.com*
[d]*Department of Chemistry and Chemistry Institute for Functional Materials, Pusan National University, Busan, 609 735, Korea. E-mail: hssuh@pusan.ac.kr*

† Electronic supplementary information (ESI) available: Synthesis of compounds, molecular dynamics simulations, Raman spectra of hollow DC and DC/Au particles, the EDX spectrum of DC/Ni(II) assemblies, and the plots of ethylene polymerization rate *versus* time. See DOI: 10.1039/c1jm13081a

This journal is © The Royal Society of Chemistry 2011

View Article Online

Published on 12 October 2011. Downloaded by York University on 22/10/2014 13:03:49.

which not only can accommodate *in situ* generated metal nanoparticles, but allow coordination of late-transition metals (such as nickel, cobalt, *etc.*) to form bulky catalysts for olefin polymerizations, few explorations have been involved. Targeted to that, herein, a novel type of multifunctional supramolecular hosts has been fabricated using α-diimine compound (DC) as building blocks (Fig. 1).

DC contains a conjugated acenaphthylene-1,2-diimine center substituted by bis(2,6-diisopropylaniline), four hydroxyl, two amine and two methoxy groups, which may facilitate the formation of promising self-assembled architectures through intermolecular π–π stacking interaction and hydrogen bonds. Multiple hydroxyl group containing compounds, such as ethylene glycol,[9] glucose[10] and hyperbranched polyglycidol,[11] can be used as effective reducing agents towards various metal ions, yielding metal nanoparticles. Analogously, DC self-assemblies contain a large number of phenolic hydroxyl groups, which may provide promising platforms for *in situ* generation and accommodation of metal nanoparticles (NPs). In addition, since the α-diimine center of DC provides reactive sites for easily coordinating late-transition metals,[12,13] each DC assembly composed of numerous building blocks can incorporate stoichiometric amount of metals, forming bulky catalysts towards olefin polymerizations.

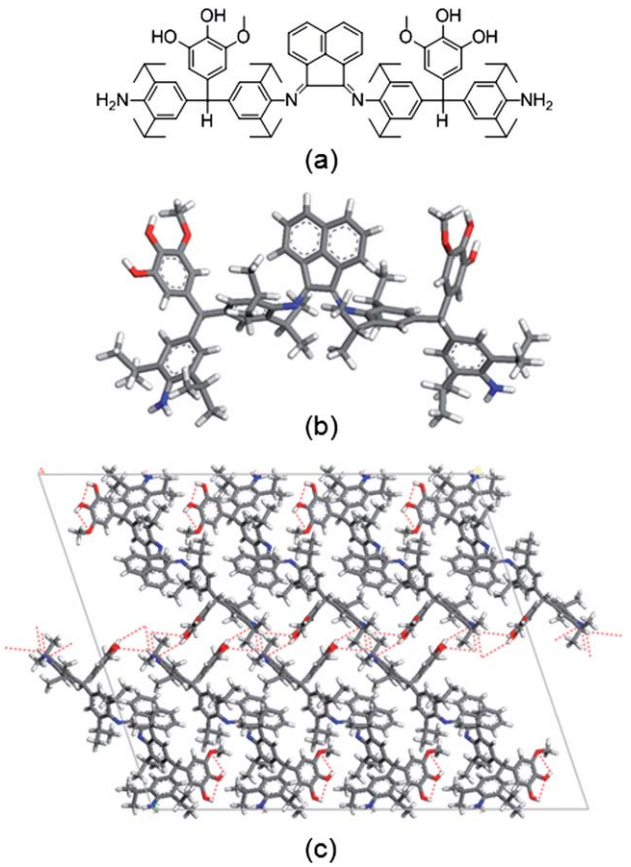

Fig. 1 (a) Molecular structure of α-diimine compound of this study; (b) its geometrical energy minimized structure generated by the Forcite model with the Dreiding 2.21 force field system and Gasteiger charges using Materials Studio™ release 4.3 (see ESI† for details); and (c) predicted crystal structure (space group = *P*1, $a = 9.752$ Å, $b = 11.597$ Å, $c = 37.867$ Å, $\alpha = 9.752°$, $\beta = 11.597°$, $\gamma = 77.5°$, density = 1.046 g cm^{-3}) by Polymorph Predictor embedded in the same package, showing a hydrogen-bonded chain (dotted line).

Experimental

Materials

The polymerization grade of ethylene (SK Co., Korea) was purified by passing it through columns of Fisher RIDOX™ catalysts and molecular sieve 5 Å/13×. All other reagents used in the current study were purchased from Aldrich Chemical Co. The organic solvents for synthesis of DC and ethylene polymerization were purified using known procedures and stored over molecular sieves (4 Å). The other chemicals were used as received without further purification.

Synthesis of DC

The synthetic procedures[13] for DC are described in the ESI†.

Fabrication of DC self-assemblies with tunable morphologies

To fabricate solid spheres, 2.0 mL of premixed solvent (THF : DI water = 1 : 3) was added to a vial containing 1 mg of DC with vigorous stirring at room temperature. Subsequently, the homogeneous solution was transferred to a cellulose acetate dialysis tube (MWCO 12 000 g mol^{-1}) and subjected to dialysis treatment in deionized (DI) water for 24 h. The obtained turbid solution was collected and the solid assembled spheres with 604 nm in average diameter were prepared. Following similar procedures, the solid assembled spheres with 183 and 115 nm in mean size were fabricated by using 0.7 and 0.4 mg of DC, respectively. To fabricate DC assembled tubes, 1.5 mL of DI water was added to a vial containing 1 mg of DC. After sonicating treatment for 30 seconds, 0.5 mL of THF was added with vigorous stirring. Thereafter, an additional 0.5 mL of DI water was injected with magnetic stirring for 5 min. Followed by dialysis treatments for 24 h, turbid assembled tubes solution was obtained. If the employed amount of additional DI water was 1.0 mL, the hollow assembled spheres can be generated following the same procedures. Note that all the DC self-assemblies were finally collected and redispersed in 2 mL of DI water.

In situ synthesis of DC/Au NPs hybrids

1.5 mL of DI water was added to a vial containing 1 mg of DC. After sonicating treatment for 30 seconds, 0.5 mL of THF was added with vigorous stirring. Thereafter, an additional 1.0 mL of $HAuCl_4$ aqueous solution (1 mM) was injected with magnetic stirring for 3 h. Followed by dialysis treatments in DI water for 24 h, solid DC/Au hybrid nanospheres dispersed in 2 mL of DI water were obtained. To fabricate hollow DC assemblies encapsulating Au NPs, hollow assembled spheres were firstly prepared as described above. Thereafter, 1.0 mL of $HAuCl_4$ aqueous solution (1 mM) was injected into the as-prepared turbid solution. After stirring at room temperature for 3 h, Au NPs were *in situ* generated and encapsulated into the matrices of hollow architectures. The resulting hybrids were purified by three-circles of centrifugation and redispersion in DI water.

View Article Online

Published on 12 October 2011. Downloaded by York University on 22/10/2014 13:03:49.

Eventually, the hollow DC/Au hybrids were collected by centrifugation and then redispersed in 2 mL of DI water.

DC self-assemblies hosting nickel ions for ethylene polymerization

Following the same procedures described above, 11.5 mg of hollow and solid DC self-assemblies were firstly prepared and redispersed in absolute ethanol, respectively. Subsequently, 2.2 mg of $NiBr_2$ (1 : 1 equivalent DC) was added into the as-prepared colloid solution. After continuous stirring at 30 °C for 24 h, the Ni(II) coordinated DC self-assemblies were purified by three-circles of centrifugation and redispersion in absolute ethanol. The solid sample was collected by centrifugation and then dried under vacuum at 60 °C overnight. Since Ni(II) coordinated DC is paramagnetic, a high resolution NMR spectroscopic analysis was not feasible. Anal. Calcd for hollow Ni(II) coordinated self-assemblies: C, 66.72; H, 6.89; N, 3.99. Found C, 66.68; H, 6.91; N, 4.05%. MS (FAB^+): m/z = 1323 (M^+ − Br). Anal. Calcd for solid Ni(II) coordinated self-assemblies: C, 66.72; H, 6.89; N, 3.99. Found C, 66.70; H, 6.91; N, 4.07%. MS (FAB^+): m/z = 1323 (M^+ − Br).

The ethylene polymerizations were carried out under a purified nitrogen atmosphere using the Schlenk technique.[13] Briefly, Ni(II) complex (2.5 μmol) and dry toluene (80 mL) were added into a 250 mL round-bottom Schlenk flask equipped with a magnetic stirrer and a thermometer outside. After the solvent was saturated with ethylene at 1.3 atm, methylaluminoxane (MAO, MAO/Ni = 250) was injected into the reaction system. The polymerization reaction was performed at 50 °C for 30 min. The reaction was stopped by the addition of ethanol. After precipitation of reaction solution in 10% HCl–EtOH and subsequent filtration, polyethylene (PE) was collected by filtration and then dried in vacuum at 40 °C for 20 h.

Characterization and molecular dynamics simulations

The ^{1}H-NMR, ^{13}C-NMR spectra of ligands were recorded on a Varian Gemimi-2000 (300 MHz, 75 MHz) spectrometer. The ^{1}H-NMR spectra of polyethylene (PE) were taken in $C_6H_4Cl_2$ at 135 °C on a Varian Unity Plus (300 MHz) spectrometer. Samples dispersed in DI water for scanning electron microscopy (SEM) were mounted onto a silicon plate and dried in air. After osmium coating was carried out with an Edwards S150B sputter coater, SEM analysis was carried out using a JSM-6700F microscope at an accelerating voltage of 10 kV. Samples dispersed in DI water for transmission electron microscopy (TEM) were deposited onto carbon-coated copper electron microscope grids and dried in air. The size, shape and fine structures of hybrids were investigated using a MODEL H-7600 (HITACHI) low resolution and a JEOL 1200 EX high resolution TEM. UV-vis absorption spectra of the samples were recorded at room temperature on a UV-1650PC apparatus (SHIMADZU). Fourier transform (FT)/Raman spectra were recorded at a resolution of 4 cm^{-1} with a Bruker IFS 66 interferometer coupled to a Bruker FRA 106 Raman module equipped with a continuous He/Ne laser. The structures of the products were examined by X-ray diffraction (XRD) with an automatic Philips powder diffractometer using a nickel-filtered CuKa radiation. The diffraction pattern was collected in the 2θ range 15–90° in steps of 0.02° and a counting time of 2 s per step.

Crystal structure prediction was performed using the Polymorph Predictor (PP) module in Materials Studio™ release 4.3. The DC molecule was first energetically optimised in the Dreiding 2.21 force field by using the Forcite model. The details are described in the ESI†.

The molecular weight and polydispersity index (PDI) of PE were determined by gel permeation chromatography (GPC, PL-GPC220/FTIR, 135 °C) in 1,2,4-trichlorobenzene using polystyrene columns as the standard. The intrinsic viscosity was measured in decalin at 135 °C using an Ubbelohde viscometer and the viscosity average molecular weight (M_v) was calculated. Differential scanning calorimetry (DSC, Perkin-Elmer) analysis was carried out at a 10 °C min^{-1} heating rate under a nitrogen atmosphere. The branching numbers for PE were determined by ^{1}H NMR spectroscopy using the ratio of the number of methyl groups to the overall number of carbons and are reported as branches per thousand carbons.

Results and discussion

DC self-assemblies with tunable morphologies

Inspired by the fabrication of DC supramolecular hosts, bare organic matrices in the form of micro- and nano-architectures were initially investigated and prepared by nonsolvent (DI water) induction phase separation from homogeneous α-diimine solution (in tetrahydrofuran (THF)), followed by dialysis treatments in DI water. More interestingly, the morphologies of resulting architectures could be effectively tuned from solid spheres, tubes to capsules by simply changing the fabrication conditions. To obtain solid spheres, DC was directly dissolved in premixed solvent of THF and DI water (v/v, 1 : 3, 0.55 mM of DC) with vigorous stirring at room temperature, followed by dialysis treatment in DI water. The resulting colloids were subjected to SEM and TEM analysis. It was observed that the yielded DC self-assemblies are solid spheres with a rather broad size distribution ranging from 200 to 2080 nm in diameter (604 nm in mean size, Fig. 2a). Following the similar fabrication procedures, when the employed concentration of DC was further decreased to 0.33 and 0.11 mM, both yielded DC assemblies exhibited solid and spherical architectures (Fig. 2b and c) with diameter in the range of 78–413 nm (183 nm in mean size) and 74–185 nm (115 nm in mean size), respectively (Fig. 2d). It can be seen that the lower employed DC concentration is favorable for the formation of DC self-assemblies with smaller size and narrower size distribution.

Upon feeding 0.5 mL of additional DI water into 2 mL of DC solution in premixed solvent of THF and DI water (v/v, 1 : 3, 0.55 mM of DC) with vigorous stirring, the homogeneous solution suddenly became turbid, indicating a rapid formation of DC self-assemblies. After dialysis against DI water, surprisingly, uniform nanotubular architectures with 100 nm of average diameter were obtained (Fig. 3a). A detailed inspection of the SEM images showed the presence of cracks in some of these nanotubes (Fig. 3b), most likely caused by the rapid evaporation of the encapsulated solvent.[14,15] The average wall thicknesses of the nanotubes were measured to be ~25 nm. Following the similar procedures for fabricating DC nanotubular architectures,

 This journal is © The Royal Society of Chemistry 2011

View Article Online

Published on 12 October 2011. Downloaded by York University on 22/10/2014 13:03:49.

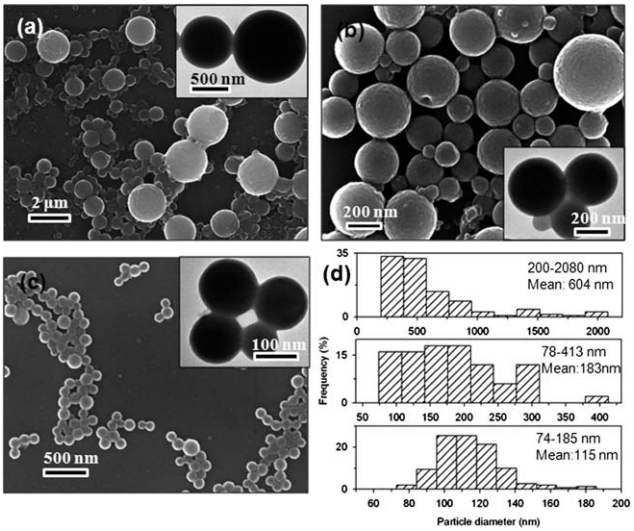

Fig. 2 SEM and TEM images of DC assemblies prepared with different concentrations of DC solutions in premixed solvent of THF and DI water (v/v, 1 : 3): (a) 0.55, (b) 0.33, (c) 0.11 mM and (d) particle size distributions of DC assemblies obtained at 0.55 (top), 0.33 (middle) and 0.11 mM (bottom).

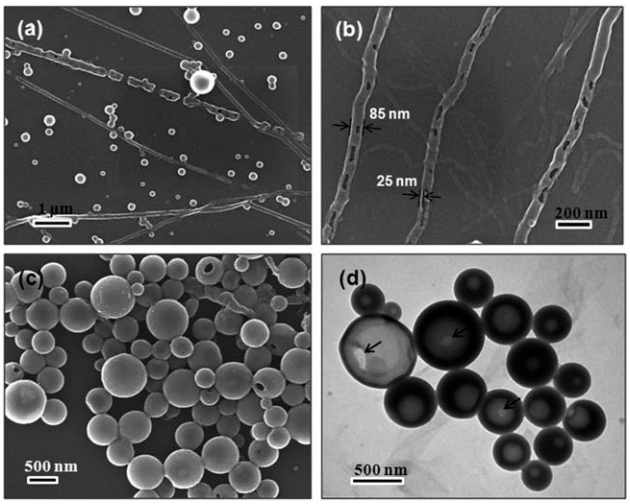

Fig. 3 (a) and (b) SEM images of DC assemblies obtained by using 0.55 mM of DC solution in THF and water (v/v, 1 : 4); (c) and (d) SEM and TEM images of hollow DC spheres prepared with 0.55 mM of DC solution in THF and water (v/v, 1 : 5).

when the employed amount of additional DI water was increased to 1.0 mL, hollow DC microspheres were achieved (Fig. 3c and d). The outer and inner diameters of these hollow spheres were 430 and 205 nm on average. In addition, the presence of a hole in some hollow spheres was also visualized as in the case of nanotubes.

As described above, the self-assembled DC architectures with tunable morphologies ranging from solid spheres, tubes to capsules can be generated by simply controlling the composition of mixed solvent and the involvement of a suitable amount of DI water. The intriguing behavior of these DC self-assemblies leads us to get insight into the key intermolecular interactions that resulted in the final self-assembled architectures. As is shown in Fig. 4a, the homogeneous DC solution shows a broad absorbance band centered at around 510 nm. Upon self-assembly, the absorbance peaks of the DC nanotubes, capsules and solid spheres are red-shifted to 550, 552 and 610 nm, respectively. These significant red shifts evidence the presence of strong intermolecular π–π stacking interactions within the DC assemblies.[16,17] In addition, compared with the shoulder band of DC solution at shorter wavelength, the DC assemblies exhibit relatively enhanced absorbance intensity, which results from the delocalization of the excited state due to π–π interaction.[16] Also, a line broadening of the absorbance bands is visualized for the DC assemblies, reflecting the strong intermolecular electronic interactions of the close-packed molecules.[18]

Further insights into the intermolecular interactions are obtained by means of Raman spectra (Fig. 4b). DC solution in the mixed solvent of THF and water shows strong bands at 2968 and 2881 cm^{-1}, corresponding to CH_3 and CH stretching vibrations, respectively. Upon self-assembly, both bands significantly red-shift and evolve into a relatively broad band situated at 3330 cm^{-1}. This red-shift of the band position and the bandwidth broadening could be related to the combined effects of the intermolecular hydrogen bondings and π–π stacking interactions.[19–21] However, the specific mechanism still remains unclear so far. Additionally, in the region of 1680–1300 cm^{-1}, DC solution exhibits strong bands ranging from 1491 to 1454 cm^{-1},

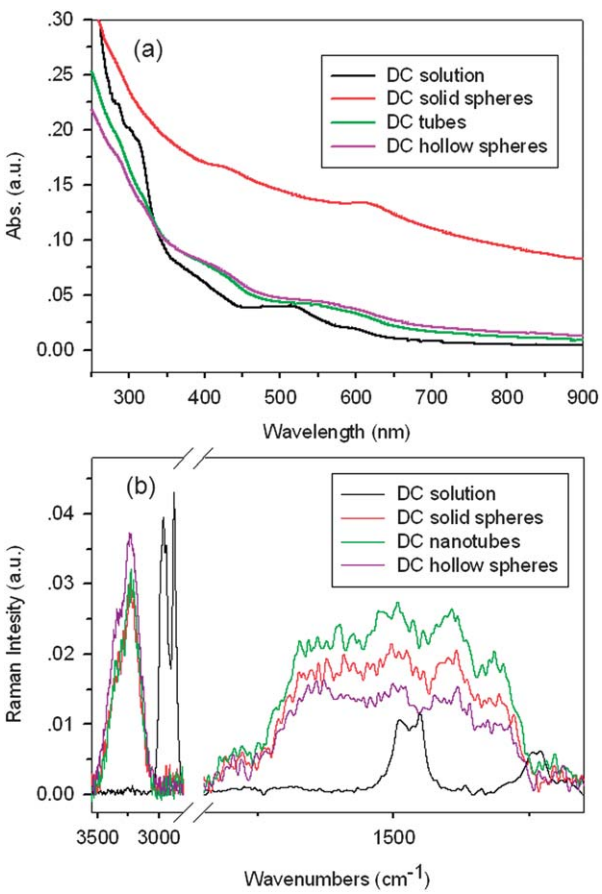

Fig. 4 (a) UV-vis and (b) Raman spectra of DC solution in the mixed solvent (THF and water, v/v, 1 : 1) and DC self-assembly colloids in water.

View Article Online

Published on 12 October 2011. Downloaded by York University on 22/10/2014 13:03:49.

characteristic of aromatic stretching modes, while the DC self-assembled colloids demonstrate more abundant bands. In the case of DC hollow spheres, the aromatic stretching vibrations red-shift to the region of 1505–1477 cm^{-1} together with newly appeared bands at 1659 and 1597 cm^{-1}, suggesting a rearranged orientation in close-packing manners of aromatic rings in the DC assemblies.[22] The bands at 1642 and 1628 cm^{-1}, 1426 and 1327 cm^{-1} are attributed to the hydrogen-bonded NH_2 and OH deformation, respectively.[23] The bands at 1383 and 1313 cm^{-1} correspond to CH_3 symmetric deformation and COH bending vibrations, respectively.[23] These results demonstrate the presence of strong hydrogen bonds in the DC assemblies, which play important roles in directing the self-assembly of DC molecules (Fig. 1). In comparison, the other DC assemblies exhibit similar Raman spectra to the DC solid spheres, although there exist slight differences in the Raman shifts and intensities, which could be caused by differences in the stacking manners of DC molecules and thus result in the formation of DC assemblies with varied morphologies.

DC/Au NPs hybrids

In order to demonstrate the efficiency of the *in situ* generation and encapsulation of metal NPs in assembled DC architectures, we first identified DC capsules as typical hosts to encapsulate Au NPs *via* a two-step process. Aqueous $HAuCl_4$ solution was added in the as-prepared self-assembled DC capsules (Fig. 3c) with sustained stirring at room temperature for 3 h in the absence of any other additional reagents. After three circles of centrifugation and redispersion in DI water, the resulting colloids were collected and subjected to microscopy examination. As is shown in Fig. 5a, the as-prepared colloids exhibit slightly rougher surfaces compared with the original DC capsules, while the size remains unchanged. The Au NPs with 9.0 nm in average diameter are clearly distinguished and randomly distributed on the shell of DC capsules (Fig. 5b). Powder XRD measurements (Fig. 5c) further evidence the successful generation of face-centered cubic structured Au NPs (JCPDS 4-784), while DC capsules exhibit a typical amorphous structure. The formation of amorphous DC assemblies is caused by the non-ordered packing of DC molecules during the self-assembly process, where the self-assembly occurs so rapidly that DC molecules are unable to adjust their configurations to orderly pack into a well-defined crystalline structure.

To further simplify the preparation procedures, we have explored a one-pot protocol to encapsulate Au NPs in the matrix of DC self-assemblies. In a typical procedure, 1.0 mL of aqueous $HAuCl_4$ solution (1 mM) was fed to 2 mL of DC solution in a premixed solvent of THF and DI water (v/v, 1 : 3, 0.55 mM of DC) with continuous stirring at room temperature for 3 h, followed by dialysis treatment in DI water. The resulting colloids exhibit uniform nanospheres with 100 nm in average diameter (Fig. 5d). More interestingly, these as-prepared nanospheres exhibit solid structures, in which numerous Au NPs are *in situ* generated. In addition, there exists a uniform shell with ~6.0 nm in thickness around the as-formed Au NPs (Fig. 5e), directly visualizing the successful encapsulation of Au NPs within the matrices of DC self-assemblies. These facts evidence the formation of DC/Au NPs solid hybrid nanospheres. The size of *in situ* formed Au NPs is ~5.5 nm in average diameter, which is smaller than the Au NPs in DC/Au capsules generated by the two-step process.

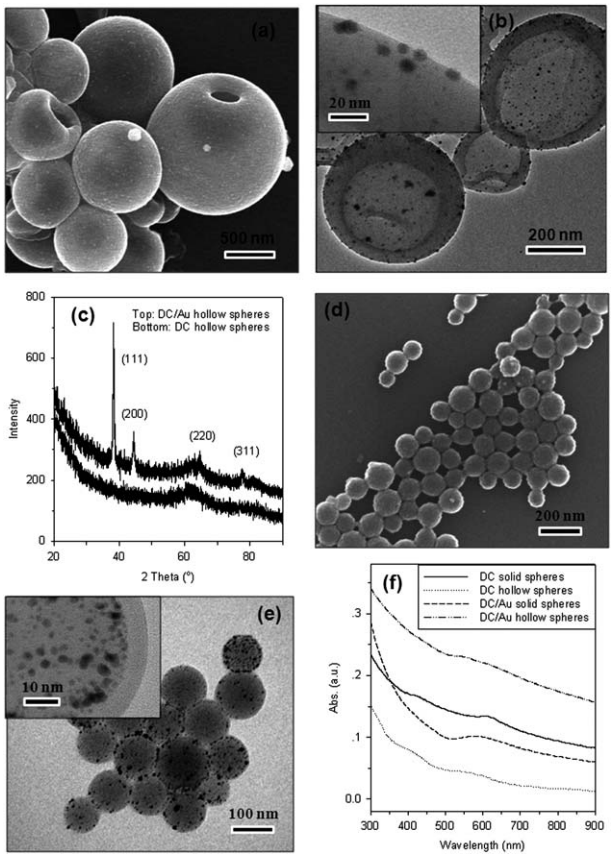

Fig. 5 (a) SEM and (b) TEM images of hollow DC/Au nanostructures; (c) XRD patterns of DC and DC/Au hollow spheres; (d) SEM and (e) TEM images of solid DC/Au nanospheres; (f) UV-vis spectra of as-prepared DC assemblies and DC/Au nanostructures.

The optical properties of the DC/Au NPs hybrids were investigated. In comparison with the UV-vis spectra of bare solid and hollow DC spheres, solid and hollow DC/Au NPs hybrid colloids exhibit a newly broad absorbance band centered at around 590 and 540 nm (Fig. 5f), respectively, corresponding to the surface plasma resonance (SPR) band of encapsulated Au NPs. Generally, free spherical Au NPs with <20 nm of average diameter show UV-vis absorbance band at around 520 nm. These significant red-shifts are characteristic of Au NPs interacted in string-like fashions,[24] evidencing the encapsulation of Au NPs within the DC self-assemblies.

In both two-step and one-pot fabrication processes, Au NPs in DC/Au NPs hybrid are *in situ* obtained in the absence of any additional reducing agents; thus DCs serve as both reducing and stabilizing agents for the *in situ* formed Au NPs. The formation of such Au NPs could follow an analogous polyol process. The polyol process has been widely explored for the synthesis of metal NPs although there is insufficient understanding of their formation mechanism.[25–27] Previous reports have revealed that the reduction of metal ions in a typical polyol process occurs only when the employed alcohols are present in high concentrations above a threshold value due to their limited reducing capability.[28]

 This journal is © The Royal Society of Chemistry 2011

View Article Online

Published on 12 October 2011. Downloaded by York University on 22/10/2014 13:03:49.

From this point of view, in the matrix of DC capsules, there are lots of hydroxyl group aggregates derived from adjacent assembled DC molecules. Each aggregate provides a "domain" with a certain alcohol concentration, which mimics an analogous polyol environment. When the metal precursor is added to self-assembled DC colloids solution, there exist non-covalent, electrostatic (ion dipole) interactions among the electropositive metal ions and electron-rich oxygen atoms in those "domains".[11,29] Such interactions cause the metal ions to be tightly trapped within the matrix of DC assemblies, forming DC/metal ions complexes. After a polyol process, these trapped metal ions were *in situ* reduced to their zero-valent metallic states, and then coalesce into metal NPs.

Note that the one-pot reaction for fabricating DC/Au NPs solid nanospheres is exactly same as the one for preparing DC capsules (Fig. 3c and d) except for the involvement of $HAuCl_4$. This can be related to the DC-assisted reducing processes of Au(III) ions, which alter the self-assembly behavior of DC molecules. This effect is evidenced by the Raman scattering measurements shown in Fig. 6. Compared with DC capsules, DC/Au solid spheres show a significantly weakened intensity of Raman bands in the region of 1800–1200 cm^{-1}, including hydrogen-bonded NH_2, aromatic stretching vibrations, hydrogen-bonded OH, CH_3 symmetric deformation and COH bending vibrations. It indicates that the number of hydrogen bonds in the DC/Au solid spheres is greatly reduced. In contrast, the band at 1596 cm^{-1} is relatively enhanced, which can be derived from the formation of Au^0–O bonds.[30] In current self-assembly processes, the hydrogen bonds serve as critical media to manipulate the intermolecular stacking, leading to the formation of various assembled architectures. However, when the aqueous $HAuCl_4$ solution is involved in the homogeneous DC solution in THF and DI water, metal ions rapidly complexed with DC molecules through the non-covalent, electrostatic interactions among the electropositive metal ions and electron-rich oxygen atoms.[29,30] This unavoidably hinders the formation of hydrogen bonds and leads to the reduction in the number of hydrogen bonds. These effects together with π–π stacking interactions direct DC to self-assemble in certain manners, resulting in the formation of DC/Au solid spheres after the reduction of complexed Au(III) ions.

In comparison with solid DC/Au particles, the incorporation of *in situ* generated Au NPs into the shell of hollow DC self-assemblies (hollow DC/Au, Fig. 5a and b) also aroused the similar changes in the Raman spectrum (Fig. S3 in the ESI†). Hence, the *in situ* reduction of Au(III) ions also results in the formation of Au^0-O bonds (1596 cm^{-1}) at the cost of the destruction of partial hydrogen bonds. Such Au^0-O bonds are beneficial for the tight trapping of *in situ* formed Au NPs within the matrix of DC assemblies.

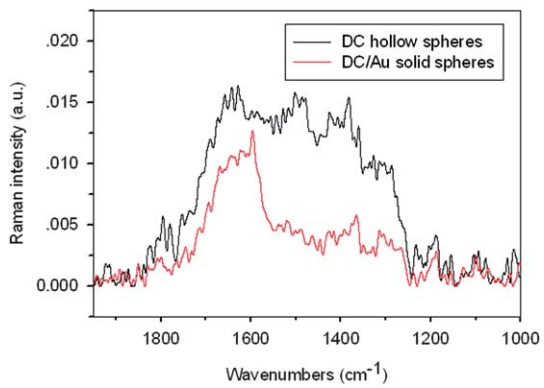

Fig. 6 Raman spectra of self-assembled DC hollow spheres and DC/Au solid spheres obtained by one-pot reaction.

Ni(II) coordinated DC self-assemblies for ethylene polymerization

The α-diimine center in DC molecules provides efficient "active sites" for coordinating late transition metals such as Ni(II) and Pd (II), forming metal complexed DCs, which are well-known efficient catalysts towards the polymerizations of diverse olefins.[12,13] Analogously, by coordinating late transition metals to the assembled DC hosts, efficient catalysts for olefin polymerizations are expected. Bulky Ni(II) α-diimine catalysts (BNDC; Fig. 7a) were fabricated by coordinating $NiBr_2$ to pre-formed hollow and solid spherical DC assemblies. Energy-dispersive X-ray analysis evidenced the presence of Ni elements in DC assemblies (Fig. S4 in the ESI†). Elemental and MS (FAB^+) analyses further confirmed the successful coordination of Ni(II) to the matrixes of DC assemblies (see Experimental section). The BNDCs keep the hollow structures and no obvious changes in morphologies after metallation reactions (Fig. 7b). These hollow BNDCs showed

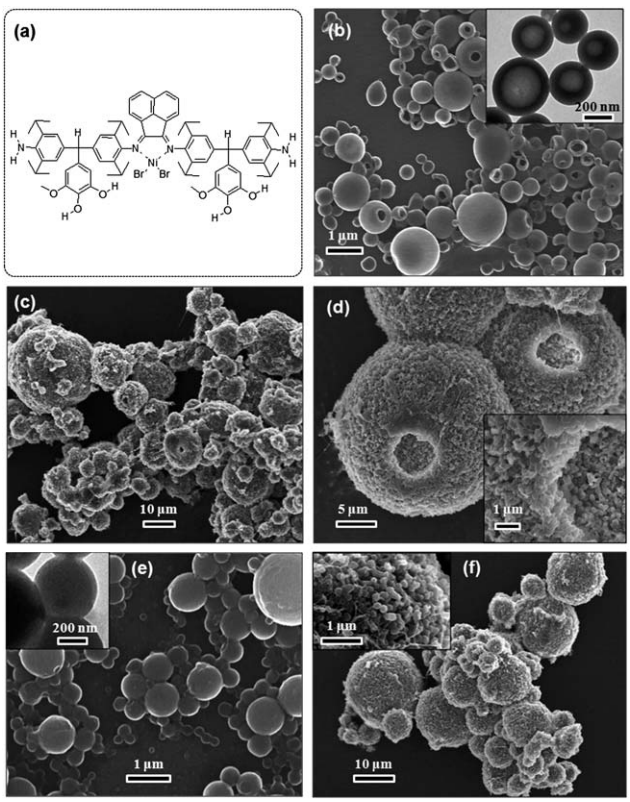

Fig. 7 (a) Molecular structure of BNDC; (b) SEM and TEM images of BNDC hollow spheres; (c and d) SEM images of PE beads polymerized by using BNDC hollow spheres as bulky catalysts; (e) SEM and TEM images of BNDC solid spheres; (f) SEM images of PE beads obtained by using BNDC solid spheres as bulky catalysts.

View Article Online

Published on 12 October 2011. Downloaded by York University on 22/10/2014 13:03:49.

excellent catalytic reactivity towards the ethylene polymerization (6.06×10^5 g PE mol Ni^{-1} h^{-1} bar^{-1}; Table 1, also see Fig. S5 in the ESI†) combined with MAO as a cocatalyst. More interestingly, the yielded polyethylene (PE) exhibits spherical structures with diameters in the range of 3.1–24.3 μm (7.4 μm in mean size, Fig. 7c), which is significantly larger than BNDCs (430 nm in average diameter). The PE beads exhibit solid structures formed by an agglomerate of large numbers of uniform PE microspheres with around 200 nm of average diameter (Fig. 7d). This fact is responsible for the rough surface of polyethylene spheres. Interestingly, it is visualized that there exists a round "trap" on the surfaces of some PE beads, exactly replicating the structures of some hollow BNDCs (Fig. 6a).

In addition, the solid BNDCs exhibit solid and spherical structures (Fig. 7e), which are similar to the original DC hosts (Fig. 2a). These BNDCs also showed good catalytic activity for ethylene polymerization assisted with MAO (1.22×10^5 g PE mol Ni^{-1} h^{-1} bar^{-1}, Table 1, also see Fig. S5 in the ESI†). The yielded PE beads show solid structures with mean sizes ranging from 2.4 to 17.8 μm (7.0 μm in average, Fig. 7f). Each PE bead consists of numerous uniform PE microspheres with 190 nm in average diameter. Interestingly, in comparison with the PE beads obtained by hollow BNDCs, no round "trap" is observed on the surfaces of yielded PE beads. This suggests that the produced PE beads replicate the surface morphologies of original solid BNDCs.

The formation of these fascinating PE structures can be explained by an analogous "multigrain model" mechanism.[31] Each building block, the Ni(II) α-diimine complex, in BNDCs acts as an active site. Since BNDCs possess textural pores formed in the self-assembly processes of DC molecules, ethylene monomers and co-catalysts are allowed to diffuse to the active sites and *in situ* polymerize, producing a large number of grain-sized polymer spheres. Accompanied with the successive feeding of monomers, polymerizations continuously occur on the living chains surrounded on the surfaces of as-formed grain-sized polymer spheres. These newly formed polymer chains push the previous formed polymer layer, thus leading to the growth of the grain-sized polymer spheres into microspheres and consequently the formation of the final PE beads. Since each building block serves as a separated active site to catalyze the production of a PE microsphere, the uniform *in situ* growth of these PE microspheres is responsible for the yield of final PE beads with replicating topology of original BNDCs. If hollow interiors in BNDCs exist, the growing PE microspheres would occupy the interior space of BNDCs, yielding the final solid PE beads. Additionally, the hollow structures of BNDCs are more favorable for the substance diffusion, giving slightly higher catalytic activity of hollow BNDCs than that of solid BNDCs. Note that the resultant PE beads possess textural pores derived from the interparticle spacing, which not only lower the density of PE materials, but also provide promising applications in the field of substance transportation. In addition, it could be feasible to generate PE beads with desired surface morphologies by using BNDCs with designed topologies. To the best of our knowledge, this is the first report concerning the achievement of PE beads with porous textures and possibly tunable surface morphologies.[32]

Table 1 Selected ethylene polymerization results[a]

Catalysts (BNDC)	$R_{p,avg}$[b] × 10^4	M_v[c] × 10^4	M_n[d] × 10^3	PDI[d]	T_m[e]/°C	Branches[f]/1000 C
Hollow DC sphere	60.6	10	43	3.8	125	37
Solid DC spheres	12.2	12	48	4.4	127	30

[a] *Conditions*: toluene = 80 mL, P_{C2H4} = 1.3 bar, catalyst = 2.5 μmol, time = 30 min, temperature = 50 °C, and MAO/Ni = 250. [b] Average rate of polymerization as g PE mol Ni^{-1} h^{-1} bar^{-1}. [c] Viscosity-average molecular weight characterized with viscometry at 135 °C in decalin (Ubbelohde viscometer). [d] Number-average molecular weight (M_n) and polydispersity index (PDI) determined by GPC. [e] Melting point determined by DSC. [f] Branches per 1000 carbon atoms determined by ^{1}H NMR.

Conclusions

A facile route to fabricate DC self-assemblies with tunable morphologies ranging from solid spheres, nanotubes and capsules *via* π–π stacking and hydrogen bond interactions has been demonstrated. The DC assemblies are excellent multifunctional hosts for *in situ* generation and encapsulation of Au nanoparticles, yielding novel solid and hollow DC/Au hybrid nanospheres by one-pot or two-step fabrication process. Solid and hollow DC assemblies were also used to host Ni(II) ions to generate DC/Ni(II) hybrid particles, resulting in bulky and highly active catalysts for ethylene polymerizations to produce porous PE beads consisting of numerous PE microspheres. Moreover, the PE beads replicate the surface morphologies of original bulky catalysts. The formation mechanism of the PE beads is elucidated as an analogous "multigrain model". Note that these DC assemblies can be used to host various metal species to fabricate a variety of DC/metal NPs (Ag, Pt, Pd, *etc.*) hybrid nanomaterials and polymer (PE, polypropylene, *etc.*) beads with porous textures.

This work was supported by the *World Class University Program* (no. R32-2008-000-10174-0), the *National Core Research Center Program* from MEST (no. R15-2006-022-01001-0), and the *Brain Korea 21 program* (BK-21).

Notes and references

1 A. Walther, J. Yuan, V. Abetz and A. H. E. Müller, *Nano Lett.*, 2009, **9**, 2026.
2 M. Schmittel and V. Kalsani, *Top. Curr. Chem.*, 2005, **245**, 1.
3 M. D. Pluth and K. N. Raymond, *Chem. Soc. Rev.*, 2007, **36**, 161.
4 C. M. Drain, A. Varotto and I. Radivojevic, *Chem. Rev.*, 2009, **109**, 1630.
5 I. Imaz, J. Hernando, D. Ruiz-Molina and D. Maspoch, *Angew. Chem., Int. Ed.*, 2009, **48**, 2325.
6 A. Ajayaghosh and V. K. Praveen, *Acc. Chem. Res.*, 2007, **40**, 644.
7 M. D. Pluth, R. G. Bergman and K. N. Raymond, *Acc. Chem. Res.*, 2009, **42**, 1650.
8 S. M. Biros, R. G. Bergman and K. N. Raymond, *J. Am. Chem. Soc.*, 2007, **129**, 12094.
9 Y. Sun and Y. Xia, *Science*, 2002, **298**, 2176.
10 P. Raveendran, J. Fu and S. L. Wallen, *J. Am. Chem. Soc.*, 2003, **125**, 13940.
11 H. Li, J. K. Jo, L. Zhang, C.-S. Ha, H. Suh and I. Kim, *Langmuir*, 2010, **26**, 18442.
12 G. G. Hlatky, *Chem. Rev.*, 2000, **100**, 1347.
13 B. K. Bahuleyan, G. W. Son, D. W. Park, C. S. Ha and I. Kim, *J. Polym. Sci., Part A: Polym. Chem.*, 2008, **46**, 1066.

 This journal is © The Royal Society of Chemistry 2011

View Article Online

14 H. Li, C.-S. Ha and I. Kim, *Langmuir*, 2008, **24**, 10552.
15 I. Alfonso, M. Bru, M. I. Burguete, E. García-Verdugo and S. V. Luis, *Chem.–Eur. J.*, 2010, **16**, 1246.
16 M. Huang, U. Schilde, M. Kumke, M. Antonietti and H. Cölfen, *J. Am. Chem. Soc.*, 2010, **132**, 3700.
17 H. Huo, K. Li, Q. Wang and C. Wu, *Macromolecules*, 2007, **40**, 6692.
18 Y. Luo, J. Lin, H. Duan, J. Zhang and C. Lin, *Chem. Mater.*, 2005, **17**, 2234.
19 T. P. Ruiz, M. F. Gómez, J. J. L. González and A. E. Koziol, *Chem. Phys.*, 2006, **320**, 164.
20 Y. Yu, K. Lin, X. Zhou, H. Wang, S. Liu and X. Ma, *J. Phys. Chem. C*, 2007, **111**, 8971.
21 D. Baskaran, J. W. Mays and M. S. Bratcher, *Chem. Mater.*, 2005, **17**, 3389.
22 R. S. Armstrong, L. M. Atkinson, E. Carter, M. S. Mahinary, B. W. Skelton, P. Turner, G. Wei, A. H. White and L. F. Lindoy, *Proc. Natl. Acad. Sci. U. S. A.*, 2002, **99**, 4987.
23 G. Socrates, in *Infrared and Raman Characteristic Group Frequencies: Tables and Charts*, ed. G. Socrates, John Wiley and Sons Ltd, 3rd edn, 2001, pp. 51, 97–99 and 107.
24 R. Djalali, Y.-F. Chen and H. Matsui, *J. Am. Chem. Soc.*, 2002, **124**, 13660.
25 L. Poul, N. Jouini and F. Fiévet, *Chem. Mater.*, 2000, **12**, 3123.
26 G. Viau, P. Toneguzzo, O. Acher, F. Fiévet-Vincent and F. Fiévet, *Scr. Mater.*, 2001, **44**, 2263.
27 S. E. Skrabalak, B. G. Wiley, M. Kim, E. V. Formo and Y. Xia, *Nano Lett.*, 2008, **8**, 2077.
28 T. Sakai and P. Alexandridis, *J. Phys. Chem. B*, 2005, **109**, 7766.
29 C.-H. Lai, I.-C. Wu, C.-C. Kang, J.-F. Lee, M.-L. Ho and P.-T. Chou, *Chem. Commun.*, 2009, 1996.
30 J.-P. Sylvestre, S. Poulin, A. V. Kabashin, E. Sacher, M. Meunier and J. H. T. Luong, *J. Phys. Chem. B*, 2004, **108**, 16864.
31 T. F. McKenna and J. B. P. Soares, *Chem. Eng. Sci.*, 2001, **56**, 3931.
32 B. K. Bahuleyan, B. C. Son, Y. S. Ha, S. H. Lee, H. Suh and I. Kim, *J. Mater. Chem.*, 2010, **20**, 7150.

Published on 12 October 2011. Downloaded by York University on 22/10/2014 13:03:49.